No. 68-666

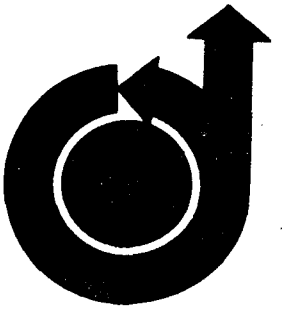

PHOTOEXCITATION AND PHOTOIONIZATION OF ARGON AHEAD OF A STRONG SHOCK WAVE

by

RICHARD A. DOBBINS
California Institute of Technology
Pasadena, California

AIAA Paper
No. 68-666

AIAA Fluid and Plasma Dynamics Conference

LOS ANGELES, CALIFORNIA/JUNE 24-26, 1968

PHOTOEXCITATION AND PHOTOIONIZATION OF ARGON AHEAD OF A STRONG SHOCK WAVE*

Richard A. Dobbins**

California Institute of Technology

Pasadena, California

Abstract

A chemical kinetic model describing photochemical reactions that are likely to be important in "cold" argon ahead of a strong shock wave is examined on a quantitative basis. The model includes the propagation of resonance radiation far from the shock front in the wings of the resonance absorption line, partial trapping of the absorbed resonance radiation, subsequent photoionization of excited atoms, photoionization of ground state argon, and certain recombination and deexcitation processes. Specific consideration is given to shock tube geometry, the occurrence of both nonequilibrium and equilibrium regions of variable lengths behind the pressure discontinuity, and the (experimentally) known shock tube wall reflectivity. Theoretical predictions of electron and excited atom concentrations ahead of the shock wave are presented for typical shock tube operating conditions.

I. Introduction

The observation of precursor ionization ahead of strong shock waves in argon contained in shock tubes in which the driver is a compressed light gas is now well documented.† Two of the earlier reports on electron precursors that appeared almost simultaneously were by Weymann[1] and by Gloerson[2], and the former credits R. M. Hollyer as being the first to describe precursors in an unpublished report dated May, 1957. Since that time, there has been experimental progress toward defining the events on a quantitative basis. Probably one of the more carefully conducted experimental studies of the electron concentration ahead of a shock wave in argon in a gas-driven shock tube is that of Lederman and Wilson[3], whose measurements were made with a tuned microwave cavity.

In the period intervening between the dates of the work of Weymann and Lederman and Wilson there have been many theoretical studies attempting to explain these observations. Physical mechanisms first proposed were photoelectric effect and diffusion of electrons from behind the shock front[1, 2]. Wetzel[4] concluded that gradient type diffusion of electrons could not produce the effects that had been observed. He later suggested that photoionization of ground state argon could be the the important mechanism[5] and this mechanism has been further analyzed by Clarke and Ferrari[6].

Photoionization of ground state argon fails to explain the occurrence of electrons far from the shock front because the photon mean free path for radiation of the relevant frequency is too small to produce the observed effects. This type of photoionization requires low densities to propagate large distances, whereas the experiments indicate that precursors are most pronounced at higher densities. On the other hand, the resonance line radiation emitted by the hot gas can propagate very large distances in the wings of the resonance absorption line in the cold gas. Once a photon of resonance radiation is absorbed, it will soon be reemitted with high probability near the center of the line where the photon mean free path is again very small and its escape to the wall of the shock tube is unlikely. This latter condition is referred to as the trapping of radiation. Thus, the combination of the propagation of energy in the wing of the resonance line combined with subsequent trapping provide a mechanism that can operate to cause electronic excitation at distances far ahead of the shock wave.

The literature of the Russian investigators in this area has recognized these concepts from the outset. Biberman and Veklenko[7], as early as 1960, predicted electronic "excitation temperature" one meter ahead of the shock wave only slightly less than the equilibrium temperature behind the shock wave. Lagar'kov and Yakubov[8] proposed in 1962 that photoionization of excited argon would lead to appreciable concentrations of electrons ahead of the shock wave. Tumakaev and Luzovskaya[9] described in 1965 what appears to be the first test of the prediction of electronically excited species ahead of the shock wave. In a similar vein, S. S. R. Murty[10] recently examined the role of line radiation on precursor ionization. His model was a shock wave of infinite extent in a hydrogenic gas, and it included the occurrence of radiation trapping.

We wish to study the precursors that have been observed in argon with the context of a kinetic model that includes the aforementioned effects. In almost all previous studies of shock wave precursors and structure, the waves have been considered to be infinite in extent. This one-dimensional approximation is totally unsuitable when radiation and radiation trapping are brought into consideration, and we wish to describe shock-tube experiments on a quantititative basis. Our model should take advantage of the relative abundance of information available on argon that has originated from studies in gaseous discharges, electron beams, and arc jets. Our aim is to seek new approaches for future experiments and to shed light on previous experiments. We note that no study of high-temperature shock structures can be realistic unless the description of the precursor is properly understood.

---

* Work supported by the Air Force Office of Scientific Research (OAR) under Contract AF 49(638)-1285.

** Presently Visiting Associate in Jet Propulsion, Guggenheim Jet Propulsion Center, California Institute of Technology; on leave of absence from Division of Engineering, Brown University, Providence, Rhode Island.

† A large body of literature on the occurrence of precursors in electrically-driven shock tubes is excluded from consideration.

$$K_0^{(i)} = \frac{S^{(i)}}{\alpha_d^{(i)}} \left(\frac{\ln 2}{\pi}\right)^{1/2} \tag{15}$$

We evaluate the above integral by means of the computer program given by Armstrong[17] using spectroscopic constants cited in Table I. We also evaluate the normalized intensity and the local absorption (excitation) rate using the limiting case of $\alpha_d^{(i)} \to 0$, $X_\nu^2 >> Y_\nu^2$ when the important absorption occurs in the dispersion-broadened line profile and the Voigt function reduces to

$$K_\nu^{(i)}/K_0^{(i)} = \frac{Y_\nu^{(i)}}{\pi^{1/2} (X_\nu^{(i)})^2} \tag{16}$$

We find that Eq. (16) accurately represents the absorption coefficient that is given more precisely by Eq. (11) except in the core of the line where no long-range transmission of energy occurs. In Figure 5 we show the normalized local intensity, $I_\nu(0)/B_\nu(T^{(2)})$, and also the local absorption (excitation) rate $K_\nu'' I_\nu(x')/B_\nu(T^{(2)})$ for a slab of gas at pressures and temperatures that can be achieved in the shock tube.

From Figure 5 we see that the intensity at the interface, $x'/L_2 = 0$, is the blackbody intensity over the entire frequency span over which absorption occurs in the cold gas, except for the largest value of x'/L_2. If the temperature discontinuity were caused by normal shock wave, a Doppler effect would occur that would shift the line center frequencies of the emission and absorption lines with respect to one another. For velocities of interest here, the frequency shift, $\Delta\nu/\nu_{21}$, would amount to less than 10^{-6}, which is very small compared to the width of the emission line in the hot gas. Thus, we may proceed to calculate the photoexcitation rate ahead of a shock wave on the basis that absorption occurs in the wing of the pressure-broadened dispersion line, that Doppler shift is negligible, and that the hot gas emits almost as a black body. We will eventually wish to improve the latter approximation to achieve better accuracy.

We now proceed to evaluate the photoexcitation rate by evaluating the number of photons absorbed per unit volume in the frequency interval surrounding ν_{21}. This rate, referring now to the notation of Figure 1, is

$$Q_{12} = 4\pi \int_{\nu_{21}-\Delta}^{\nu_{21}+\Delta} \frac{K_\nu^{(i)} J_\nu(\eta)}{h\nu} d\nu \tag{17}$$

where the specific spectral average intensity is given by

$$J_\nu(\eta) = \frac{1}{4\pi} \int I_\nu(\eta, \omega) d\omega \tag{18}$$

Treating the equilibrium zone as a blackbody emitter at the upstream equilibrium temperature, we have, for the local specific spectral intensity,

$$I_\nu(\theta, x') = B_\nu(T^{(2)}) \exp(-K_\nu x' \sec\theta) \tag{19}$$

In expressing the radiation intensity in the form given by Eq. (19), we have neglected reemission in the cold gas. Thus, we have treated the radiative transfer equation as $dI_\nu/ds = -K_\nu I_\nu$ and integrated directly. The neglect of the emission term in the gas ahead of the shock wave can be justified a posteriori, and this approximation will be used throughout this work, which is concerned with early precursor effects. The approximation is expected to fail near to the pressure discontinuity and also in both the non-equilibrium and equilibrium regions behind the pressure discontinuity.

We substitute (19) into (18) and convert solid angle to polar angle θ and we obtain

$$J_\nu(x') = \frac{B_\nu(T^{(2)})}{2} \int_0^{\theta_c} \sin\theta \exp(-K_\nu^{(i)} x' \sec\theta) d\theta \tag{20}$$

We obtain the average specific spectral intensity by the substitution $z = \sec\theta$ and $\eta = x'/R$, in the following form:

$$J_\nu(\eta) = \frac{B_\nu(T^{(2)})}{2} \left\{ E_2(K_\nu'' R\eta) - (1+\eta^{-2})^{-1/2} E_2[K_\nu''(1+\eta^{-2})^{1/2}] \right\} \tag{21}$$

where

$$E_2(\chi_\nu) = \int_1^\infty \frac{\exp(-\chi_\nu z)}{z^2} dz \tag{22}$$

The photoexcitation rate can be expressed as

$$Q_{12} = \frac{2\pi}{\eta} \frac{B_\nu(\nu_{21}, T^{(2)})}{h\nu_{21}} \int_{\nu_{21}-\Delta}^{\nu_{21}+\Delta} \chi_\nu \left\{ E_2(\chi_\nu) - (1-\eta^{-2})^{-1/2} E_2[\chi_\nu(1+\eta^{-2})^{1/2}] \right\} d\nu \tag{23}$$

where χ_ν is the spectral optical depth, $K_\nu R$. In Eq. (23) we have removed quantity $B_\nu(\nu, T^{(2)})/h\nu_{21}$ from under the integral sign because of its relatively slow variation with frequency over the range $\nu_{21} \pm \Delta$. To evaluate the integral we use Eq. (16) for K_ν and convert the integration variable to $1/s = (\nu - \nu_{21})^2/\alpha_L^2(\pi\alpha_L/\eta R)$. We find

$$Q_{12} = \frac{2\pi}{\eta} \frac{B_\nu(\nu_{21}, T^{(2)})}{h\nu_{21}} \left(\frac{S^{(i)} \alpha_L^{(i)} \eta R}{\pi}\right)^{1/2} \times \int_{s_0}^\infty \left[\frac{E_2(s)}{s^{1/2}} - (1-\eta^{-2})^{-1/2} \frac{E_2(z_0 s)}{s^{1/2}} \right] ds \tag{24}$$

Finally, by interchanging the order of integration with respect to angle and frequency, we obtain

$$Q_{12} = \frac{4\pi}{3} B_\nu(\nu_{21}, T^{(2)}) \left(\frac{\alpha_L^{(i)} S^{(i)}}{R}\right)^{1/2} f(\eta) \tag{25}$$

where

$$f(\eta) = \eta^{-1/2} \left[1 - (1+\eta^{-2})^{-3/4} \right] \tag{26}$$

We note that for $\eta \gg 1$ the shock front emits as a point source and we have

$$f(\eta \gg 1) = 3/4\ \eta^{-2.5}$$

Thus, we see that at large η, the excited specie generation rate, or local photon absorption rate, decreases as $\eta^{-0.5}$ due to absorption and as η^{-2} due to geometric attenuation. A correction to the geometric factor will be made later to account for shock-tube wall reflections.

2. De-excitation by Spontaneous Emission with Radiation Trapping

An excited atom will exist prior to decay to the ground state for an average period of time that is simply the reciprocal of the spontaneous emission rate, A_{21}, given by the Einstein theory of radiation[20]. This spontaneous emission rate is

$$A_{21} = \frac{8\pi^2 e^2 g_1 f}{m_e c \lambda_{21}^2 g_2} \qquad (27)$$

At pressures as low as 10^{-3} atmospheres, the photon emitted by the de-excitation process will be absorbed with high probability in a distance very small compared with the radius of a shock tube. Thus, many successive absorption and re-emission processes are required before the photon created in the original de-excitation process reaches the wall. The process is referred to as radiation trapping, and it has been extensively studied in this country by Holstein[21-23], Phelps[24], and their colleagues as well as by Biberman[25, 26] and his coworkers in Russia. Holstein (Ref. 22, Eq. 6.6) has calculated the probability of escape of trapped radiation of a photon when the dominant line-broadening mechanism is the (low) pressure broadening in the dispersion portion of the line profile. Using the Fursov-Vlassov relation, Eq. (10), for the Lorentz semi-half width, we express Holstein's result as

$$g_{t2} = \frac{1.115}{3^{1/2}\pi}\left(\frac{\lambda_{21}}{R}\right)^{1/2} = 0.205\left(\frac{\lambda_{21}}{R}\right)^{1/2} \qquad (28)$$

The effective de-excitation rate is simply the product of Eqs. (27) and (28). Radiation trapping theory is well developed, and the theory has successfully described the limited number of experiments that have been performed.

3. Photoionization of Excited Argon

The local rate of photoionization of excited argon is found by evaluating the local rate of absorption of photons in frequency range $\nu_{i2} \le \nu < \infty$. That is,

$$Q_{2i} = 4\pi \int_{\nu_{i2}}^{\infty} \frac{\sigma_2(\nu)\, J_\nu(\nu, T^{(2)})}{h\nu}\, d\nu \qquad (29)$$

We consider the possibility that radiation in both the ν_{i2} and ν_{21} frequency ranges can photoionize the excited argon. We therefore divide the frequency range of the integration indicated in Eq. (29) into two intervals which will be evaluated separately.

$$Q_{2i} = Q_{2i}'(\nu_{i2}) + Q_{2i}'' = 4\pi \int_{\nu_{i2}}^{\nu_{i2}+\Delta} \frac{\sigma_2(\nu_{i2})\, J(\nu_{i2}, T^{(2)})}{h\nu}\, d\nu$$

$$+ 4\pi \int_{\nu_{21}-\Delta}^{\nu_{21}+\Delta} \frac{\sigma_2(\nu_{21})\, J(\nu_{21}, T^{(2)})}{h\nu}\, d\nu \qquad (30)$$

The photoionization cross section of excited argon is given by Schlüter[27] in the following form

$$\sigma_2(\nu) = \frac{64\pi^4 m_e e^{10} \lambda^3 g_{f2}(n^*, \epsilon)}{3\sqrt{3}\, c^4 h^6 n^{*5}} \qquad (31)$$

where the Gaunt factor $g_{f2}(n^*, \epsilon)$ depends on the effective principal quantum number, n^*, and also the electron energy, ϵ, given by

$$\epsilon = \frac{1}{R_y \lambda} - \frac{1}{n^{*2}} \qquad (32)$$

For the ν_{i2} cutoff frequency of the $^1P_1$ state of argon I, Schlüter[27] gives $n^* = 1.8197$ and $g_{f2}(n^*, 0) = 0.01195$. With these numbers we find the photoionization cross section to be 1.67×10^{-19} cm^2, which is in general agreement with an estimate of this cross section given by Lagar'kov and Yakubov[8]. The cross section at higher frequencies is then expressed as

$$\sigma_2(\nu > \nu_{i2}) = \sigma_2(\nu_{i2})\left(\frac{\nu_{i2}}{\nu}\right)^3 \frac{g_{f2}(\nu')}{g_{f2}(\nu_{i2})} \qquad (33)$$

where

$$\sigma_2(\nu_{i2}) = 1.67 \times 10^{-19}\ \text{cm}^2.$$

We proceed to evaluate the intensity of the average spectral specific radiative intensity for the ν_{i2} spectral region. We note that it is well established that the optical depth in this spectral region is small compared with unity. By this we mean that self-absorption in the hot gas behind the equilibrium front is negligible, and hence absorption in the cold gas, except by excited atoms, is totally absent. Equation (7) can be applied for the local specific spectral intensity in the form obtained by taking $K_\nu^{(2)} L_2 \ll 1$ and $K_\nu^{(1)} X' \ll 1$

$$I_\nu(\eta, \theta) = K_\nu^{(2)} L_2 \sec\theta\, B_\nu(\nu, T^{(2)}) \qquad (34)$$

We determine the average intensity at a point on the axis of a right circular cylinder a distance η cylinder radii from the equilibrium front. The result of the calculation is

$$J_\nu(\nu, T^{(2)}) = \frac{1}{4} B_\nu(\nu, T^{(2)}) K_\nu L_2\, g(\eta) \qquad (35)$$

where

$$g(\eta) = 2\left\{\left[\frac{1}{\gamma}(\theta_2 - \theta_1) - \eta \ln\frac{\sec\theta_2}{\sec\theta_1}\right] + \ln\sec\theta_1\right\} \qquad (36)$$

and $\cos\theta_1 = \left[1 - (\eta + \gamma)^{-2}\right]^{-1/2}$ $\cos\theta_2 = (1 + \eta^{-2})^{-1/2}$

$\gamma = L_2/R$ and $\eta = x'/R$

When $\psi \approx \eta$ and $\eta \gg 1$, then the terms in the square bracket vanish and we have $g(\eta \gg 1) \rightarrow \eta^{-2}$. Thus, at large distances from the shock front, we recover the inverse square law geometric attenuation for the spectral intensity of the secondary continuum, which is not strongly absorbed in either the hot or cold gas.

The atomic absorption coefficient in the region behind the equilibrium front, $K_\nu^{(2)}$, is given by the following equations[28-30], very similar to a corresponding relation due to Unsold

$$K_\nu = 6 A_1 \frac{n_i^2 h^3}{c^3 h} \exp\left(-\frac{h\nu_{i1}}{kT}\right)\left[\exp\left(\frac{h\nu}{kT}\right)-1\right] \bar{g}(\nu, T) \quad (37)$$

with

$$A_1 = \frac{32 \pi^2 e^6}{3\sqrt{3}\, h^3 c^3} \quad (38)$$

In Eq. (37) we have approximated the ratio of the statistical weights of the ion and atom as 6.0. The factor $\bar{g}(\nu, T)$ represents the quantum mechanical correction factor for departure from hydrogenic behavior.

By combining the Planck function

$$B_\nu(\nu, T) = \frac{2h\nu^3}{c^2}\left[\exp\left(+\frac{h\nu}{kT}\right)-1\right]^{-1} \quad (39)$$

with Eq. (37) multiplied by the ground state atom concentration in the hot gas equilibrium zone, $n_{a1}^{(2)}$, we obtain the product of the Planck function and the absorption coefficient as

$$B_\nu(\nu, T) K_\nu = 12 A_1 n_{a1}^{(2)} k T^{(2)} \exp\left(-\frac{h\nu_{i1}}{kT^{(2)}}\right) \bar{g}(\nu, T^{(2)}) \quad (40)$$

We insert Eqs. (36) and (40) into the first integral to obtain

$$Q'_{2i}(\nu_{i2}) = A_2 L_2 n_{a1}^{(2)} f(T^{(2)}) \sigma_2(\nu_{i2}) g(\eta) \quad (41)$$

where

$$f(T^{(2)}) \equiv T^{(2)} \exp\left(-S_{i1}^{(2)}\right) \Omega_2(T^{(2)})$$

and

$$\Omega_2(T^{(2)}) \equiv 3 \int_1^\infty \left(\frac{\nu_{i2}}{\nu}\right)^4 \frac{g_{f2}(\nu)}{g_{f1}(\nu_{i2})} \bar{g}(\nu, T^{(2)}) d\left(\frac{\nu}{\nu_{i2}}\right) \quad (42)$$

and

$$A_2 = \frac{128 \pi^3 e^6 k}{3\sqrt{3}\, c^3 h^4} = 2.494 \times 10^{24} \ \text{erg}^{-1}\,\text{sec}^{-1} \quad (43)$$

In the hydrogenic approximation $\bar{g}(\nu, T)$, $g_{f2}(\nu)$, and $\Omega_2(T^{(2)})$ are all equal to unity. In our calculations, we use Schlüter's values of the $\bar{g}(\nu, T)$ function which do not involve the use of a cutoff frequency. A revised calculation of the $\bar{g}(\nu, T)$ factor has been completed by Schlüter[31] and some values appropriate to the ν_{i2} frequency range are quoted, along with values of $g_{f2}(\nu)$, in Table II. Using these quantities, we find the Gaunt integral can be expressed as

$$\Omega_2(T^{(2)}) = 0.194\left(\frac{T^{(2)}}{10^4}\right) - 0.065 \quad (44)$$

In using Schlüter's $\bar{g}(\nu, T)$ factor, we are including the effect of radiation formed not only by recombination to the first excited state, but also to all higher states when an electron possesses sufficient energy to give rise to radiation in the ν_{i2} frequency range. Thus, while our model accounts for only a single excited state in the cold gas, we do include the effect of all excited states in the hot gas when the spectral quality of the emitted radiation is calculated. It is important to include these components of radiation in the ν_{i2} frequency range because of the small value of the absorption (emission) cross section, $\sigma_2(\nu_{i2})$.

The second integral in Eq. (30) is evaluated by using Eq. (33) for the photoionization cross section of excited argon and Eq. (21) for the average intensity of radiation. The result is

$$Q''_{2i}(\nu_{i2}) = 4\pi \frac{B_\nu(\nu_{i1}, T^{(2)})}{h\nu_{21}} \sigma_2(\nu_{i1}) \Delta_e h(\eta) \quad (45)$$

where

$$h(\eta) \equiv \frac{1}{\Delta_e}\left[\int_{\nu_{i1}}^{\nu_{i1}+\Delta} E_2(K\beta'' R\eta) \frac{I_\nu}{B_\nu} d\nu - (1+\eta^{-2})^{-1/2} X\right] \quad (46)$$

and

$$\int_{\nu_{i1}}^{\nu_{i1}+\Delta} E_2\left[K\beta'' R\eta (1+\eta^{-2})^{1/2}\right] \frac{I_\nu}{B_\nu} d\nu\Bigg]$$

$$I_\nu / B_\nu = 1 - \exp\left(-K_\nu^{(2)} L_2\right) \quad (47)$$

In Eq. (45), we have taken the frequency dependent factors that are slowly varying outside of the integral which has a frequency range limited to the width of the emission line in the hot gas. This portion of the calculation is therefore somewhat complicated by the necessity to introduce those properties of the hot gas that influence the width of the emission line. In view of Eqs. (12), (13), (15), and (16), we may express the absorption coefficient as

$$K_\nu^{(i)} = \frac{\alpha_L^{(i)} S^{(i)}}{\pi\left[\nu - \nu_{i1}\right]^2} \quad (48)$$

where i = 1, 2.

The limit of integration for the integral expressed in Eq. (46) is several times some frequency interval characteristic of the emission line width, Δ_e. The equivalent line width used by Hunt and Sibulkin[32] is convenient for this purpose,

$$\Delta_e = \left(\alpha_L^{(2)} S^{(2)} L_2\right)^{1/2} \quad (49)$$

To present Eq. (46) in a form suitable for integration, we change the integration variable to $\gamma = (\nu - \nu_{i1})/\Delta_e$ and obtain

$$h(\eta) = \int_0^{\Delta/\Delta_e} E_2(\tau_\gamma^{(i)}) f_\gamma d\gamma - (1+\eta^{-2})^{-1/2} X \quad (50)$$

$$\int_0^{\Delta/\Delta_e} E_2\left[\tau_\gamma^{(i)} (1+\eta^{-2})^{1/2}\right] f_\gamma d\gamma$$

$$f_\gamma = 1 - \exp\left(-\frac{1}{\pi\gamma^2} \frac{\alpha_L^{(i)} S^{(i)}}{\alpha_c^{(i)} S^{(i)}}\right)$$

We evaluate the integral by means of the approximation[33]

$$E_2(x) = A e^{-Bx} \quad (51)$$

where

$$A = 0.50 \qquad B = 1.35$$

Finally, we obtain

$$h(\eta) = A\left\{(BC+1)^{1/2} - (BC)^{1/2} - (1+\eta^{-2})^{-1/2} \times \right. \quad (52)$$

$$\left. [(BC'+1)^{1/2} - (BC')^{1/2}]\right\}$$

where

$$C = \frac{R}{L_2}\frac{\alpha^{(1)}S^{(1)}}{\alpha^{(2)}S^{(2)}} \qquad C' = C(1+\eta^{-2})^{1/2} \quad (53)$$

4. Photoionization of Ground State Argon

The photoionization of ground state argon is calculated by evaluating the rate of absorption of photons of sufficient energy to cause direct ionization of ground state argon. The rate of absorption of photons of frequency $\nu > \nu_{i1}$ per unit of ground state atom is

$$Q_{i1} = 4\pi \int_{\nu_{i1}}^{\infty} \frac{\sigma_i(\nu_{i1})\, J_\nu}{h\nu}\, d\nu \quad (54)$$

It is reasonable to assume the shock front emits as a black body in the spectral region $\nu_{i1} < \nu < \infty$. For the black body emission the average intensity is again given by Eq. (21).

The photoionization cross section of ground state argon has been measured by Samson[34], and over a frequency range of from $\nu_{i1} < \nu < \nu_2$, its value is close to 34×10^{-18} cm^2 where $\nu_2 \approx 1.67\nu_{i1}$. We consider the cross section to be zero beyond the frequency ν_2 and we find that the value of ν_2 is not critical. Thus, we express the direct photoionization rate as

$$Q_{i1} = 8\pi \frac{\sigma_i(\nu_{i1})}{c^2} e(\eta) f(\nu_{i1}, S_{i1}^{(1)}, \mu_2) \quad (55)$$

where

$$2e(\eta) = E_2(K_{\nu_{i1}}^{(1)} R\eta) - (1+\eta^{-2})^{-1/2} E_2\left[K_{\nu_{i1}}^{(1)} R\eta (1+\eta^{-2})^{1/2}\right] \quad (55a)$$

$$f(\nu_{i1}, S_{i1}^{(1)}, \mu_2) \equiv \int_{\nu_{i1}}^{\nu_2} \nu^2 \exp\left(-\frac{h\nu}{kT^{(1)}}\right) d\nu \quad (55b)$$

$$(55c)$$

We evaluate the above integral

$$f(\nu_{i1}, S_{i1}^{(1)}, \mu_2) = \frac{\nu_{i1}^3 \exp(-S_{i1}^{(1)})}{(S_{i1}^{(1)})^3} \times \quad K_{\nu_{i1}}^{(1)} = \sigma_i n_{i1}^{(1)}$$

$$\left\{\left[(S_{i1}^{(1)})^2 + 2S_{i1}^{(1)} + 2\right] - \exp\left[-S_{i1}^{(1)}(\mu_2 - 1)\right]\left[(S_{i1}^{(1)}\mu_2)^2 + 2S_{i1}^{(1)}\mu_2 + 2\right]\right\} \quad (55d)$$

where

$$S_{i1}^{(1)} = \frac{h\nu_{i1}}{kT^{(1)}} \quad \text{and} \quad \mu_2 = \nu_2/\nu_{i1}$$

5. Shock Tube Reflectivity Function

The photoexcitation rates given above have been calculated on the basis that no reflections occur at the shock tube walls. Visual observations of a light source placed inside a metal tube of rather low quality surface finish indicate that wall reflections can substantially augment the radiant intensity over its value in the absence of reflections. This crude test suggests tha a more quantitative evaluation of the influence of wall reflectivity may be obtained as follows. The intensity of a stable light source inside a shock tube is measured by a stable, linear photometric transducer as the distance between the source and transducer is varied. The test is then repeated with the shock tube removed and care is exercised to prevent reflections from any surface or light from any foreign source from reaching the receiver. We then define the reflectivity function, $r(\eta)$, as the ratio of the intensities measured with shock tube present to intensity measured with shock tube absent. The area of the light source should correspond to the shock tube cross section and the irradiance should be uniform across the surface of the source.

The sensitive surface of the receiver should be small with respect to the cross section of the shock tube if we wish to know the reflectivity appropriate for the shock tube centerline. Ideally, the effective frequency content of the light source should conform, in turn, to the various frequencies which cause photochemical effects. This proves nearly impossible, because the resonance radiation of argon is at a frequency where window materials and transducers are either difficult to work with or nonexistent. We have performed crude measurements of the shock tube reflectivity with two shock tube sections using a light source of one centimeter diameter, a receiver with a sensitive area of 2 cm diameter, and a monopass filter which passes radiation at 4190 Å. For a 3-inch round mild steel tube, we found the reflectivity function was approximately expressed by

$$r(\eta) = 1.11\eta - 1.0 \qquad \eta > 2 \quad (56)$$

The wall finish of the steel tube was poor because some of the corrosion that developed during storage could not be readily removed. We expect that well finished steel shock tubes will normally display a higher reflectivity than indicated by Eq. (56).

For a 2-inch square extruded aluminum shock tube that was rather heavily oxide coated, we measured a reflectivity function that was lower by a factor of 7 at large η, but still linear in η. Thus, we conclude that the numerical constant in the reflectivity function will vary over a wide range and must be measured for each particular shock tube. An approximate first power dependence of $r(\eta)$ on η is indicated by our tests.

We multiply the above photochemical reaction rates by the reflectivity function to obtain the augmented rate applicable when wall reflectivity is considered. This is conveniently performed by replacing the geometric factors, viz., $e(\eta)$, $f(\eta)$, $g(\eta)$, and $h(\eta)$ by their respective products with $r(\eta)$.

III. Conservation Equations

We calculate the electron concentration by solving the specie conservation equations for the excited atoms and electrons respectively:

$$-u_1 \frac{dn_{a2}}{dx} = +Q_{i2} - g_{t2}A_{21}n_{a2} - Q_{21}'n_{a2} - Q_{21}''n_{a2} \quad (57)$$

and

$$-u_1 \frac{dn_e}{dx} = +Q_{21}'n_{a2} + Q_{21}''n_{a2} + Q_{i1}n_{a1} \quad (58)$$

The negative sign on the left side arises because $+u_1$ and $+x$ are oppositely directed; a positive sign on the right side indicates a source term.

We nondimensionalize the equation by means of

$$\phi_2 = \frac{n_{u2}}{(n_{u2}^{(2)})_{eq}} \qquad \phi_e = \frac{n_e}{(n_e^{(2)})_{eq}} \quad \text{and} \quad \eta = x/R$$

where

$$(n_{u2}^{(2)})_{eq} = n_{u1}^{(2)} \frac{g_2}{g_1} e^{-S_{21}^{(2)}} \quad \text{and} \quad (n_e^{(2)})_{eq} = \alpha^{(2)} n_{u1}^{(2)}$$

Equations (57) and (58) become

$$\frac{d\phi_2}{d\eta} = b_1 \phi_2 - b_2 f(\eta) r(\eta) + b_3 i(\eta) r(\eta) \phi_2 + b_4 h(\eta) r(\eta) \phi_2 \qquad (59)$$

with

$$b_1 = 0.205 \left(\frac{\lambda_{21}}{R}\right)^{1/2} A_{21} \left(\frac{R}{u_1}\right) \qquad (60)$$

$$b_2 = \frac{4\pi}{3} \frac{B_\nu(\nu_{21}, T^{(2)})}{h\nu_{21}} \left(\frac{\kappa_L^{(2)} S^{(2)}}{R}\right)^{1/2} \left(\frac{R}{u_1 (n_{u2}^{(2)})_{eq}}\right) \qquad (62)$$

$$b_3 = \frac{A_2 L_2 n_{u1}^{(2)} f(T^{(2)}) \sigma_2(\nu_{21}) R}{u_1} \qquad (63)$$

$$b_4 = 4\pi \frac{B_\nu(\nu_{21}, T^{(2)}) \sigma_2(\nu_{21}) \Delta_c R}{h\nu_{21} u_1} \qquad (64)$$

and

$$\frac{d\phi_e}{d\eta} = -e_2 e(\eta) r(\eta) - e_3 g(\eta) r(\eta) \phi_2 - e_4 h(\eta) r(\eta) \phi_2 \qquad (65)$$

with

$$e_2 = \frac{8\pi \sigma_1(\nu_{21}) n_{u1}^{(1)}}{c^2} f(\nu_{21}, S_{21}^{(2)}, \mu_1) \left[\frac{R}{u_1 (n_e^{(2)})_{eq}}\right] \qquad (66)$$

$$e_3 = b_3 \frac{(n_{u2}^{(2)})_{eq}}{(n_e^{(2)})_{eq}} \qquad (67)$$

$$e_4 = b_4 \frac{(n_{u2}^{(2)})_{eq}}{(n_e^{(2)})_{eq}} \qquad (68)$$

For the quasi-steady solution, the boundary conditions are applied as follows. The equation (59) is solved for ϕ_2 assuming $d\phi_2/d\eta = 0$ at $\eta = \eta_{max}$ and that the only important terms are those representing photoexcitation $(b_2 f(\eta) r(\eta))$ and partially-trapped, spontaneous emission $(b_1 \phi_2)$. Thus, we have

$$\phi_2(\eta = \eta_{max}) = \frac{b_2}{b_1} f(\eta) r(\eta) \qquad (69)$$

When the full equation (59) is solved, we find that ϕ_2 is given with fair accuracy by Eq. (69) over a moderate range of η. Thus, the concentration of n_{u2} is primarily controlled by the photoexcitation and partially-trapped, spontaneous emission rates. This is confirmed by examination of the relative magnitudes of the other terms in Eq. (59). Furthermore, since the derivative term proves to be small, we may describe the excited state generation as purely photochemical in nature, i.e., a stationary light source of the same frequency content as the shock front would produce the same excited atom distribution. We will comment further on the implications of these results. The boundary condition for Eq. (65) is applied by setting ~~ϕ_e equal an estimated value such as $\phi_e = 0$ at $\eta = \eta_{max}$. We find that an improved estimate for ϕ_e is afforded within one iteration.~~

The value of η_{max} should correspond to the distance from the equilibrium zone at the time it is first "fully developed" to the point where measurements are performed. This distance is almost impossible to estimate, but we found that the electron concentration is not strongly sensitive to the value of η_{max}. For example, in one case, a variation of η_{max} by a factor of 2 results in a comparable change in the local value of n_e and virtually no difference in n_{u2}.

IV. Some Numerical Results

In the numerical results that are presented below, the length of the test gas region in the shock tube is given by the following dimensional expression

$$L = L_1 + L_2 = 4.84 P_1 R^2 \left(1 - \frac{m-11}{24}\right) \qquad (70)$$

where P_1 is in torr, R in cm, and L in cm. Equation (70) is developed from Mirel's theory[35] for test time in argon-filled shock tubes where, when $P_1 R \leq 6$ torr-cm, a laminar wall boundary layer persists.

The equilibration length is given by

$$\log_{10}\left(\frac{P_1 L_1}{u_1}\right) = 0.368 \times 10^{+5} \frac{1}{T_{ic}} - 8.634 - 0.00846\, \ell\ell \qquad (71)$$

where T_{ic} is the frozen flow temperature behind the pressure discontinuity, and the impurity level, $\ell\ell$, is in ppm. This equation is fitted to the theoretical predictions of Chubb[36] for pure argon and also fitted to the experimental measurements by Petchek and Byron[37] and Wong and Bershader[38] for impure argon. The importance of the value of the thickness of the equilibrium zone, L_2, indicates that this quantity can be accurately known, preferably by direct measurement.

Before we discuss some specific numerical results in detail, it is worthwhile to report some general observations.

1. We find that, for the specie concentrations and times involved, the photoexcitation and photoionization rates are high compared to collisional de-excitation and radiative-collisional recombination rates calculated when the electron temperature is assumed to be 300°K. Since these rates are fastest when the electron temperature is lowest, then neglect of these reactions is justified. The electron temperature then drops out of the problem as formulated in a single excited-state model.

2. The ratio of the photoionization rate of excited argon by resonance radiation to photoionization rate by the secondary continuum is in the range of 2 to 20 per cent for the calculations we have made. While this is small enough to ignore in our calculations, we point out that the former type of photoionization will produce electrons with about 7.9 volts of energy. Thus, photoionization of excited argon by the secondary (and primary) continuum becomes an important source of electron heat-

ing which must be considered in shock structure calculations.

3. Photoionization of ground state argon is usually very minor except at the lowest densities and highest Mach numbers. The influence of this process of electron generation was usually revealed by a sharply increased gradient in the electron concentration near the shock front.

4. The electron concentration calculated from the simultaneous equations (59) and (65) varies in direct proportion to e_3, which contains the photoionization cross section, the associated Gaunt factors, the length of the equilibrium region, a temperature dependent exponential factor, etc. Thus, an accurate knowledge of these quantities is required.

5. The reflective property of the shock tube wall is extremely important because it affects not only the generation rate of excited argon, but also the number of photons available to photoionize the excited specie. Because both of these quantities vary in direct proportion to reflectivity, the electron concentration varies as the square of the reflectivity.

6. Excited atom concentration is directly proportional to b_2/b_1 and, it appears, should be more easily predicted than electron concentration.

In Figures 6, 7, and 8, we show some excited atom and electron concentration profiles ahead of a shock wave in argon in a shock tube of one inch diameter. The impurity level, which influences excited state level only insofar as impurities affect the position of the equilibrium front, has been chosen somewhat high in order to assure the attainment of equilibrium at the lowest pressure. At the highest pressure, we violate the criterion for applicability of laminar boundary layer theory in predicting the length of the test gas L. With this exception, the calculations realistically described conditions that can be achieved in a combustion-driven shock tube. For all calculations given below, we used a value of 150 for η_{max} and the reflectivity function given by Eq. (56). Shock jump conditions were taken from De Leeuw's report[39].

In Figure 6, we show the excited atom concentration profiles at $M = 12$ for three pressures. By examination of the calculations it is possible to interpret the profiles as follows. The value of ϕ_2 is very nearly the same for all three cases because b_1 and b_2 are constant; the former identically the same in all three cases, the latter nearly so because of cancellation of changes in the exponential factor and particle densities. When n_{a2} is recovered from ϕ_2, the curves differ from one another by a factor of five due to the varying level of $(n_{a2}^{(2)})_{eq}$ as influenced by density and temperature.

Electron concentration profiles are shown in Figure 7 for the corresponding calculations. For $p_1 = 1.0$ torr, the electron concentration is in the 10^{+1} to 10^{+2} range at moderate values of η but increases very rapidly at small values of η because of the strong influence of photoionization of ground st .te argon at low pressures. The electron profiles for 3 and 10 torr differ by the product of the following influences:

(a) a factor of 5 for increased value of n_{a2},
(b) a factor of 2 increase in $f(T^{(2)})$ for a 5 per cent increase in $T^{(2)}$;
(c) a factor of 3 due to density increase,
(d) a factor of 4 due to increase in L_2.

In Figure 8 we show electron profiles for 3.0 torr pressure over a range of Mach number. In this particular case, the difference between the $M = 12$ and $M = 14$ curves appears mainly due to
(a) a factor of 4 increase in n_{a2} because of a 10 per cent increase in $T^{(2)}$; and
(b) a factor of 6 increase in $f(T^{(2)})$ for the same reason.

This theoretical model fails to predict the level of electron density that is reported from the measurements of Lederman and Wilson.[3] With the Gaunt factors and reflectivity values available, our estimates are lower than the experimental values by about 10^{+3}. The inclusion of the $^3P_1$ state would merely increase the electron concentration by a factor of two. The lack of agreement may result from a combination of factors, such as the use of a reflectivity function that is too low, the presence in the experiment of strong emission in the ν_{12} frequency range due to impurities or due to the mixing of the driver and test gas at the interface, possible nonlinearly additive effects that result when all four states in the 4s level are considered simultaneously, or other factors. The most striking feature of the experimental results is the high degree of ionization that is produced sometimes under circumstances that never permit equilibrium to be achieved behind the shock wave. Perhaps the most important result obtained from this model is the prediction of very high excited state concentrations ahead of the shock wave in a shock tube geometry.

Acknowledgment

The author is deeply indebted to Dr. Dieter Schlüter for the information generously conveyed on photoionization cross sections prior to its publication. The advice and encouragement of the staff of the Guggenheim Jet Propulsion Center, with whom the author was privileged to spend his sabbatical leave, is also acknowledged.

References

1. Weymann, H. D., "Electron diffusion ahead of shock waves in argon," Phys. Fluids 3 (1960), pp. 545-548.

2. Gloerson, P., "Some unexpected results of shock heating xenon," Phys. Fluids 3 (1960), pp. 857-870.

3. Lederman, S. and Wilson, D. S., "Microwave resonant cavity measurements of shock produced electron precursors," AIAA J. 5 (1967), pp. 70-77.

4. Wetzel, L., "Precursor effects and electron diffusion from a shock front," Phys. Fluids 5 (1962), pp. 824-830.

5. Wetzel, L., "A feature of precursor ionization profiles due to shock radiation," Phys. Fluids 6 (1963), pp. 750-752.

6. Ferrari, C. and Clarke, J. H., "On photoionization ahead of a strong shock wave," in Supersonic Flow, Chemical Processes, and

Radiative Transfer, edited by D. B. Olfe and V. Zakkay, Pergamon Press, New York (1964), pp. 375-398.

7. Biberman, L. M. and Veklenko, B. A., "Radiative processes ahead of a shock-wave front," JETP 37 (1960), pp. 117-120.

8. Lagar'kov, A. N. and Yakubov, I. T., "The effect of radiation of the state of a gas ahead of a shock-wave front," Optics and Spect. 14 (1963), pp. 103-107.

9. Tumakaev, G. K. and Lazovskaya, V. R., "Investigation of the state of mercury vapor in a shock tube by the Rozhdestvenskii hook method," Sov. Phys.-Tech. Phys. 9 (1965), pp. 1449-1455.

10. Murty, S. S. R., "Effect of line radiation on precursor ionization," JQSRT 8 (1968), pp. 531-554.

11. Zel'dovich, Ya. B. and Raizer, Yu. P., Physics of Shock Waves and High-Temperature Hydrodynamic Phenomena, Vol. I, English translation edited by W. D. Hayes and R. F. Probstein, Academic Press, New York (1966), p. 135.

12. Mitchell, A. C. G. and Zemansky, M. W., Resonance Radiation and Excited Atoms, Cambridge Press, London (1934), pp. 92-104.

13. Griem, H. R., Plasma Spectroscopy, McGraw Hill, New York (1964), p. 97.

14. Breene, R. G., Jr., "Line Width," in Handbuch der Physik, Band XXVII, Spectroskopie I, Springer Verlag, Berlin (1964), p. 56.

15. Fursov, W. and Vlassov, A., "Zur theorie der verbreiterung von spectrallinien in homogenem gaz," Phys. Zeits. Sow. 10 (1936), pp. 378-412.

16. Breene, R. G., Jr., same as reference 14 above, p. 52.

17. Armstrong, B. H., "Spectrum line profiles: the Voigt function," JQSRT 7 (1967), pp. 61-88.

18. Moore, C. E., "Atomic Energy Levels," Vol. I, N. B. S. Circular 467 (June 15, 1949), pp. 211-215.

19. Knox, R. S., "Excited-state wave functions, excitation energies, and oscillator strengths for argon ($3p^5 4s$)," Phys. Rev. 110 (1958), pp. 375-381.

20. Mitchell, A. C. G. and Zemansky, M. W., same as reference 12 above, pp. 93-97.

21. Holstein, T., "Imprisonment of resonance radiation in gases," Phys. Rev. 72 (1947), pp. 1212-1233.

22. Holstein, T., "Imprisonment of resonance radiation in gases, II," Phys. Rev. 83 (1951), pp. 1159-1168.

23. Alpert, D., McCoubrey, A. D., and Holstein, T., "Imprisonment of resonance radiation in mercury vapor," Phys. Rev. 76 (1949), pp. 1257-1259.

24. Phelps, A. V., "Effect of the imprisonment of resonance radiation on excitation experiments," Phys. Rev. 110 (1958), pp. 1362-1368.

25. Biberman, L. M., JETP 17 (1947), p. 416.

26. Biberman, L. M. and Gourevitch, I. M., "Absorption of resonance radiation and formation of metastable atoms in mercury vapor," JETP 20 (1950), pp. 108-116.

27. Schlüter, Dieter, personal communication dated 9 March 1968.

28. Biberman, L. M. and Norman, G. E., "Plasma radiation due to recombination and bremsstrahlung processes," JQSRT 3 (1963), pp. 221-245; translated as General Dynamics Report GA-tr-4943, San Diego (19 Feb. 1964).

29. Schlüter, D., "Die berechnung der ubergangswahrscheinlichkeiten von seriengaenzkontinua mit andwendung auf die schweren edelgase," Zeit. für Astrophy. 61 (1965), pp. 67-76.

30. Schlüter, D., "The calculation of bound-free transition probabilities and their applications to the continuum spectra of the rare gases," JQSRT 5 (1965), pp. 87-89.

31. Schlüter, D., personal communication dated 23 October 1967.

32. Hunt, B. L. and Sibulkin, M. S., "Radiation transfer in nitrogen for the case of uniform properties and local thermodynamic equilibrium," JQSRT 7 (1967), pp. 761-785.

33. Vincenti, W. G. and Kruger, C. H., Jr., Introduction to Physical Gas Dynamics, Wiley and Sons, New York (1965), p. 483.

34. Samson, J. A. R. S., "Experimental Photoionization cross sections in argon from threshold to 280 Å," JOSA 54 (1964), pp. 420-421.

35. Mirels, H., "Test time in low-pressure shock tubes," Phys. Fluids 6 (1963), pp. 1201-1214.

36. Chubb, D. L., "Ionizing shock structure in a monatomic gas," Report No. 34, Plasma Laboratory, School of Engineering and Applied Science, Columbia University, N. Y. (March 1967).

37. Petchek, H. and Byron, S., "Approach to equilibrium behind strong shock waves in argon," Annals of Phys. 1 (1957), pp. 270-315.

38. Wong, H., and Bershader, D., "Thermal equilibration behind an ionizing shock," J. Fluid Mech. 26 (1966), pp. 459-479.

39. DeLeeuw, J. H., "The interaction of a plane strong shock wave with a steady magnetic field," Report 49, Institute of Aerophysics, University of Toronto (March 1958).

TABLE I. Selected Energy Levels of Argon I

State	Energy[18] (cm^{-1})	Energy* (volts)	Transition Wavelength(Å)
^1S_o	0	0	0
$^1P_1$	95399.87	11.828	1048.22**
$^2P_{3/2}$	127109.9	15.7593	-

* Converted from energy given by Moore[18] in cm^{-1} by 1 volt = 8065.73 cm^{-1}.

** Theoretical[19] f no. = 0.200 .

TABLE II. Selected Gaunt Factors for Argon I

ϵ	g_{f2} for $^1P_1$ argon
0.00	0.01195
0.01	0.00955
0.04	0.00423
0.09	0.00238

λ (Å)	$\xi(\lambda, T)$ 8000°K	10000°K	12000°K
2900	0.40	0.55	0.70
2600	0.20	0.34	0.47
2300	0.10	0.19	0.30
2000	0.033	0.083	0.15

Nomenclature

A_{21} spontaneous emission probability

$B_\nu(\nu, T^{(i)})$ Planck function evaluated at temperature

c speed of light

e charge on an electron

f oscillation strength

g_1 statistical weight of ground state

g_2 statistical weight of excited state

g_{k2} Gaunt factor for photoionization cross section of excited state

g_{t2} escape probability from radiation trapping theory

G_2 Gaunt integral factor defined in text

h Planck's constant

dt impurity concentration in parts per million

I_ν specific spectral intensity

J_ν average spectral intensity

K_o absorption coefficient at center frequency of a spectral line

k Boltzmann constant

$\kappa_\nu^{(i)}$ spectral absorption coefficient

l distance between shock wave pressure discontinuity and contact surface

L_1 distance between the pressure discontinuity and the equilibrium front

L_2 distance between equilibrium front and the contact surface

M Mach number of shock wave

m_e mass of an electron

m_A mass of the atom

n_{a1} number of ground state atoms per unit volume

n_{a2} number of excited state atoms per unit volume

n_e number of electrons per unit volume

n^* effective principal quantum number

Q_{12} photoexcitation rate from state 1 to state 2

Q_{2i} photoionization rate from state 2 to state i

Q'_{2i} photoionization rate from state 2 to state i due to radiation of ν_{i2} frequency range

Q''_{2i} photoionization rate from state 2 to state i due to radiation of ν_{12} frequency range

Q_{i2} radiative collisional recombination rate

R shock tube radius

R_y Rydberg constant

$S^{(i)}$ line strength

S_{21} electron - excited atom collisional de-excitation rate

$T^{(i)}$ temperature in region i

T_{∞} frozen flow temperature behind the shock wave

u_1 velocity of gas approaching shock wave as measured in coordinates fixed in the wave

x distance from shock wave pressure discontinuity

x' distance from equilibrium front

$\alpha^{(2)}$ degree of ionization at equilibrium conditions behind the shock wave

α_d semi-half width due to Doppler broadening

α_L semi-half width due to Lorentz broadening

Δ frequency interval

Δ_e equivalent line width

ε electron energy, see text

ζ distance measured in ratio x'/R

η distance measured in ratio x/R

κ_λ absorption coefficient per atom

λ wavelength

λ_{21} wavelength corresponding to frequency ν_{21}

ν frequency

ν_{21} frequency of radiation accompanying de-excitation from excited state to ground state

ν_{i2} frequency of radiation accompanying recombination to first excited state

ν_{i1} frequency of radiation accompanying recombination to ground state

σ_1 photoionization cross section of ground state argon

σ_2 photoionization cross section of excited argon

τ_ν optical depth

ϕ_e dimensionless electron concentration

ϕ_2 dimensionless excited state concentration

x integration variable

y L_1/R

ω solid angle

Subscripts

1 ground state

2 excited state

$_{eq}$ at equilibrium conditions downstream of the shock wave

Superscripts

^{c} conditions at (1) or (2)

^{1} conditions upstream of the shock wave

^{2} equilibrium conditions downstream from the shock wave

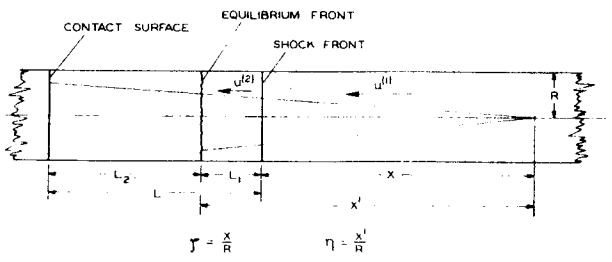

Figure 1. Length and Coordinate Definitions.

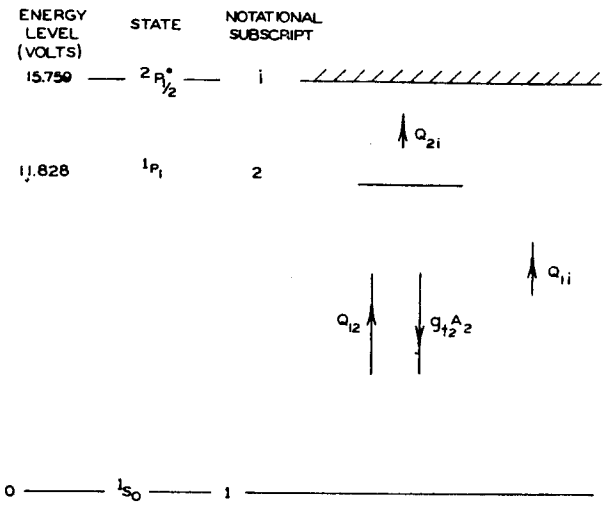

Figure 2. Simplified Energy Level Diagram.

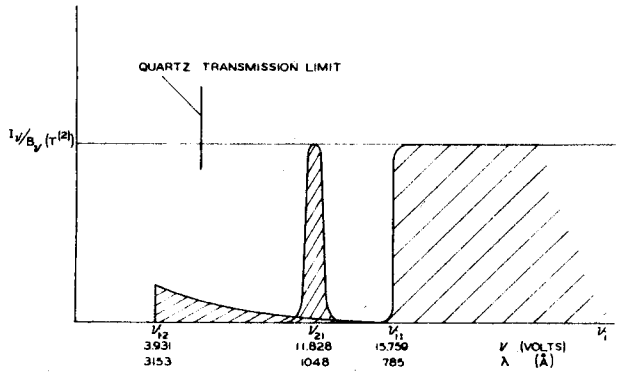

Figure 3. Schematic Diagram of Hot Gas Emission Spectrum.

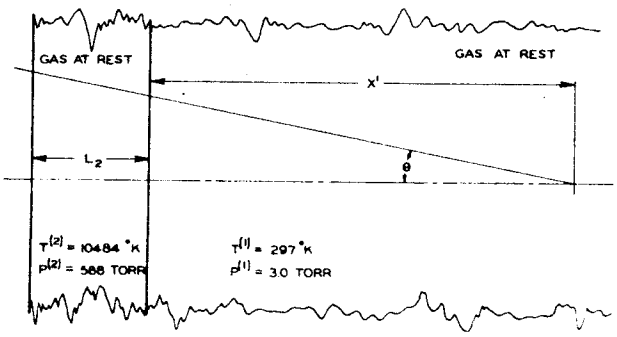

Figure 4. Radiative Transfer from a Hot Slab to a Cold Ambient Gas.

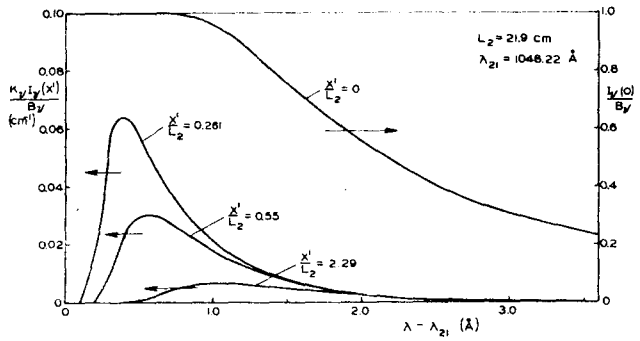

Figure 5. Hot Gas Emission and Cold Gas Local Absorption.

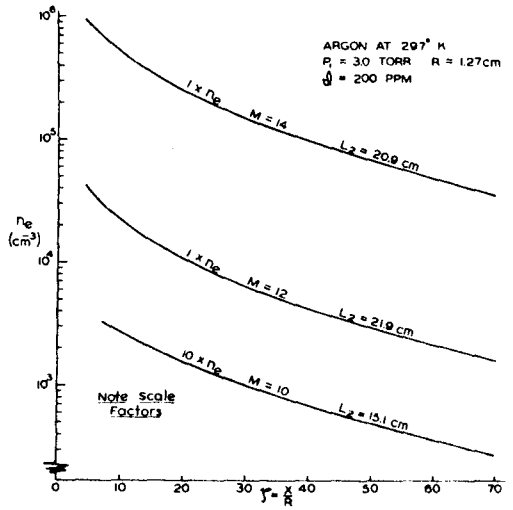

Figure 8. Electron Concentration Profiles, Constant P_1.

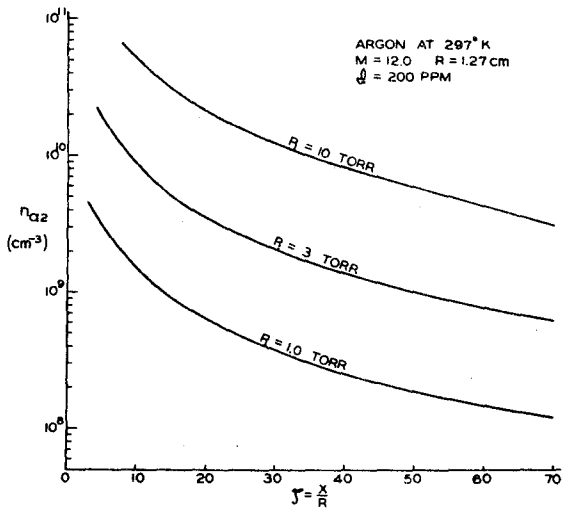

Figure 6. Excited Atom Concentration Profiles.

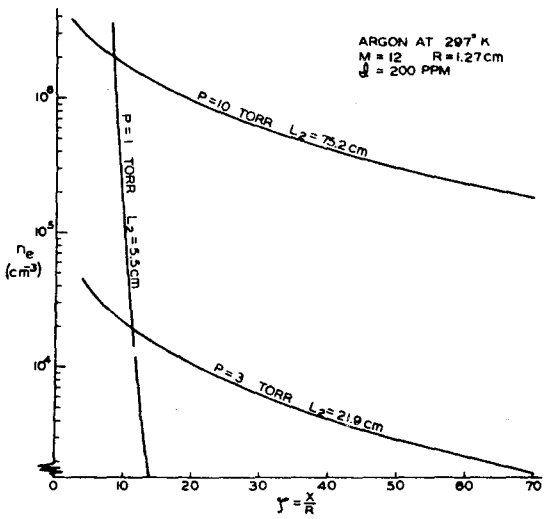

Figure 7. Electron Concentration Profiles, Constant M.